On the spatiotemporal diversity of Atlantic Niño and associated rainfall variability over West Africa and South America

Ignasi Vallès-Casanova[1,2], Sang-Ki Lee[2*], Gregory R. Foltz[2] and Josep L. Pelegrí[1]

[1]Institut de Ciències del Mar, CSIC, Unidad Asociada ULPGC-CSIC, Barcelona, Spain

[2]Atlantic Oceanographic and Meteorological Laboratory, NOAA, Miami, FL, USA

Accepted in Geophysical Research Letters

March 2020

Corresponding author address: Dr. Sang-Ki Lee, NOAA, Atlantic Oceanographic and Meteorological Laboratory, 4301 Rickenbacker Causeway, Miami, FL 33149, USA.

E-mail: Sang-Ki.Lee@noaa.gov

Abstract

The spatiotemporal evolutions of equatorial Atlantic sea surface temperature anomalies (SSTAs) during Atlantic Niño events and the associated climate impacts on the surrounding continents are extremely diverse. In this study, we construct longitude-time maps of equatorial Atlantic SSTAs for each observed Atlantic Niño event during 1948-2019, and perform a spatiotemporal empirical orthogonal function analysis to identify the four most frequently recurring Atlantic Niño varieties. The first two contrast the timing of dissipation (early-terminating versus persistent), while the other two the timing of onset (early-onset versus late-onset). Largely consistent with the differences in the timings of onset and dissipation, these four varieties display remarkable differences in rainfall response over West Africa and South America. Some of these varieties are subject to onset mechanisms that involve preconditioning in boreal spring from the Atlantic Meridional Mode or El Niño in the Pacific, while for others there is no clear source of external forcing.

Plain Language Summary

A phenomenon known as Atlantic Niño is characterized by the appearance of warm sea surface temperature anomalies (SSTAs) in the eastern equatorial Atlantic in northern summer. When it attains its full strength, it increases rainfall and the frequency of extreme flooding over the West African countries bordering the Gulf of Guinea and in northeastern South America. Atlantic Niño thus has a direct socioeconomic impact in emerging countries in these regions. However, not all Atlantic Niño events are alike. Some appear earlier than others or persists longer. These variabilities during the onset and dissipation phases are well captured by the four most recurring Atlantic Niño varieties identified in this study. Largely consistent with the differences in the timings of onset and dissipation, these four varieties display remarkable differences in rainfall response over West Africa and South America. Some of these varieties are also subject to preconditioning in northern spring by cold SSTAs in the North Atlantic or El Niño in the Pacific, while for others there is no clear source of external forcing.

- A systematic statistical analysis identifies the four most frequently recurring Atlantic Niño varieties during 1948-2019.
- Due to the differences in the timings of onset & dissipation, they display large differences in rainfall over West Africa & South America.
- Some of these varieties are preconditioned by the AMM or Pacific El Niño, while for others there is no clear source of external forcing.

1. Introduction

Perhaps the most remarkable example of tropical Atlantic atmosphere-ocean variability is the intermittent failure in the seasonal formation of the surface cold tongue, a phenomenon known as Atlantic Niño. Closely phase-locked with the seasonal cycle, Atlantic Niño usually develops in boreal spring (March-May; MAM), peaks in the summer (June-August; JJA), and dissipates in the fall. As summarized in Figure 1, Atlantic Niño is typically characterized by warm sea surface temperature anomalies (SSTAs) and positive sea surface height anomalies (SSHAs) in the eastern equatorial Atlantic, and westerly wind anomalies in the western basin (e.g., Philander 1986; Zebiak 1993; Carton and Huang 1994). Some Atlantic Niño events are also responsible for a failure of the West African summer monsoon, and increased frequency of flooding in the West African countries bordering the Gulf of Guinea and in northeastern South America (e.g., Folland et al., 2001; Giannini et al., 2003; Okumura and Xie, 2004; Losada et al., 2010; Tschakert et al., 2010; Lübbecke et al., 2018; Foltz et al., 2019). Some studies have also suggested a far reaching impact on Indian summer monsoon rainfall (e.g., Kucharski et al, 2008; Pottapinjara et al., 2019)

In many respects, Atlantic Niño is analogous to El Niño in the Pacific. As such, the leading theory behind it is an atmosphere-ocean positive feedback process known as Bjerknes feedback. Atmospheric teleconnection from the Pacific is thought to cause the westerly wind anomalies in the western basin to initiate the positive feedback (e.g., Carton and Huang, 1994; Latif and Grötzner, 2000; Chang et al., 2006; Keenlyside and Latif, 2007; Lübbecke and McPhaden, 2013; Martín-Rey et al., 2018; Tokinaga et al., 2019). More specifically, the westerly wind anomalies in the western Atlantic generate downwelling equatorial Kelvin waves that propagate to the eastern basin, deepening the thermocline and temporarily stalling (or reducing) upwelling-induced SST cooling. As a result, warm SSTAs are produced in the cold tongue region, intensifying the westerly wind anomalies via a Gill-type response (Gill, 1980) to prolong the stalling of the equatorial SST cooling (e.g., Keenlyside and Latif, 2006; Foltz and McPhaden, 2010; Lübbecke and McPhaden 2012; Burmeister et al., 2016).

However, only a fraction of the observed Atlantic Niño events can be explained by the classical Bjerknes feedback initiated by remote influence from the Pacific (e.g., Chang et al., 2006; Brandt et al., 2011; Lübbecke and McPhaden, 2012; Lübbecke et al., 2018). For instance, some Atlantic Niño events are initiated by oceanic advection of off-equatorial warm anomalies in the absence of westerly wind anomalies in boreal spring (Richter et al., 2012) or are forced by a weakening of the South Atlantic anticyclone and the associated onset of warm SSTAs in the Angola-Benguela region (e.g., Shannon et al., 1986; Florenchie et al., 2004; Lübbecke et al., 2010, 2014; Nnamchi et al., 2016). Such Atlantic Niño events preconditioned by off-equatorial processes or purely thermodynamic and stochastic processes (Nnamchi et al., 2015; Jouanno et al., 2017) are not governed by El Niño-like dynamics and thus are sometimes referred to as non-canonical events (Richter et al., 2012).

As briefly summarized above, multiple atmosphere-ocean processes are at work to trigger Atlantic Niño events. As such, the dichotomous classification of the observed Atlantic Niño events into canonical and non-canonical events often invoked in recent studies is an oversimplification. The main goal of this study is to objectively identify and explain the differences in the spatiotemporal evolution of equatorial Atlantic SSTAs and the associated rainfall variability over West Africa and South America for the entire lifespans of the events.

2. Data and Methods

In this study, we combine observational and reanalysis datasets. Monthly SSTAs are derived from three SST datasets for the 1948-2019 period: the Hadley Centre Sea Ice and SST dataset version 1 (HadISST1; Rayner et al., 2003), which is used as the primary SST dataset, the Centennial *in situ* Observation-Based Estimates of the variability of SST (COBE; Ishii et al., 2005), and the Extended Reconstructed SST version 5 (ERSST5). Monthly anomalies of surface winds (at 10 m), velocity potential and divergent winds at 200 hPa, and mean sea level pressure are from the NCEP-NCAR reanalysis (Kalnay et al., 1996) for the same period. Monthly precipitation anomalies are derived from the NOAA gauge observation-based global land precipitation reconstruction (Chen et al. 2002) for the same period. Monthly sea surface height anomalies (SSHAs), which are used here as proxies for thermocline depth anomalies, are obtained from ECMWF Ocean Reanalysis System 4 (ORAS4; Balmaseda et al., 2013) for 1958 - 2017.

Since we are mainly interested in interannual variability, a separate 30-year averaged climatology is constructed every five years and used to compute SSTAs. For instance, to compute SSTAs for the 1951-1955 period, a 30-year averaged climatology for 1936-1965 is used; to compute SSTAs for 1956-1960, a 30-year averaged climatology for 1941-1970 is used; and so forth. This method defines Atlantic Niño events by their contemporary climatology. It is also currently being used at NOAA's Climate Prediction Center to define El Niño events.

We identify 22 Atlantic Niño events, based on the threshold that the 3-month averaged SSTAs exceed 0.5°C in the ATL3 region (3S°-3°N, 20°W-0°) for at least two consecutive overlapping seasons. Warm events identified based on only one or two SST datasets are excluded to reduce uncertainties in observations. See Text S1, and Tables S1-S3 for an extended discussion of the threshold used to identify the 22 Atlantic Niño events. A longitude-time map of the equatorial Atlantic SSTAs, averaged between 3°S and 3°N, is derived for each of the 22 Atlantic Niño events. The time and longitude axes span from January to December and the entire equatorial Atlantic

(50°W-10°E), respectively. As shown in Figure S1, the spatiotemporal evolution patterns of the 22 events are different in terms of the timing, zonal extent, and amplitude of their onset, peak, and decay (e.g., Okumura and Xie, 2006; Richter et al., 2012; Marin-Rey et al., 2019). In fact, it is difficult to find any single event that can be described by the composite mean (Figure 1a) or any two events that closely resemble each other. For instance, the 1991 event peaked in May-June and dissipated very quickly afterward, followed by the onset of a cold event. In contrast, the 1963 event was very strong and persisted through the end of that year.

In order to objectively identify the preferred spatiotemporal modes of the observed Atlantic Niño events, we perform an empirical orthogonal function (EOF) analysis of these 22 longitude-time maps of equatorial Atlantic SSTAs. The resulting principal components (PCs) are associated with each individual Atlantic Niño event, and the EOFs represent a linearly independent set of longitude-time maps. The two leading PCs, which explain 30% and 24% of the inter-event variance, are further rotated by 90° to better align several observed Atlantic Niño events with the PCs. In order to better understand atmosphere-ocean processes associated with the onsets of different Atlantic Niño varieties, spatiotemporal patterns of ocean and atmospheric variables are obtained by linearly regressing the corresponding time series onto these rotated PCs. Note that the same method was previously used to identify the leading spatiotemporal modes of the observed El Niño events in the Pacific (Lee et al., 2014; 2018).

3. Four Most Frequently Recurring Atlantic Niño Varieties and Their Climate Impact on the Surrounding Continents

Each rotated EOF mode represents two contrasting Atlantic Niño varieties or flavors (rotated PC changing from -1 to 1) that correspond to adding and subtracting the rotated EOF SSTA pattern to the composite mean, leading to a total of four main Atlantic Niño varieties (Figure 2). The first rotated EOF mode distinguishes two contrasting varieties during the decay phase. As shown in Figure 2a, the first variety is characterized by a rapid and complete termination of warm equatorial Atlantic SSTAs shortly after August. It is therefore referred to as an early-terminating variety. Consistent with the early-terminating equatorial Atlantic warm SSTAs, precipitation over the West African sub-Sahel region (averaged over 0°-10°N) is enhanced mainly during July-August, although enhanced precipitation over northeastern South America (averaged over 0°-10°N) tends to persist slightly longer. It is interesting to note that precipitation over northeastern South America is reduced during April-May. Three events (1974, 1991 and 1996) appear to have the early-terminating variety (Figure 2e).

The second variety is characterized by strong equatorial Atlantic SSTAs that remain until the end of the year and is thus referred to as a persistent variety (Figure 2b). Consistent with the strong and persistent equatorial Atlantic SSTAs, precipitation over the West African sub-Sahel region is greatly enhanced for an extended period from July to October. Precipitation over northeastern South America is enhanced during September-December, supported by the persistent equatorial Atlantic SSTAs during those months. However, rainfall is much reduced in January-May, and this cannot be explained as a response to the equatorial Atlantic SSTAs. Seven events (1963, 1973, 1984, 1987, 2010 and 2016, 2019) tend to display the persistent variety (Figure 2e).

The second rotated EOF mode distinguishes two contrasting varieties during the onset phase. Following the two varieties already identified from the first rotated EOF mode, the third variety is characterized by a gradual development of equatorial warm SSTAs starting in January or earlier and is thus referred to as an early-onset variety (Figure 2c). In this case, the equatorial Atlantic warm SSTAs start to dissipate relatively early. Interestingly, the early development of equatorial

Atlantic SSTAs does not lead to increased precipitation over the West African sub-Sahel region before July. Thus, West African sub-Sahel precipitation is enhanced for a limited period mainly during July-August for the early-onset variety. Enhanced precipitation over northeastern South America during June-August is consistent with the timing of the maximum equatorial Atlantic SSTAs. However, the reduced precipitation in January-April and the enhanced precipitation in September-December cannot be explained by the equatorial Atlantic SSTAs. Rainfall anomalies over northeastern South America prior to and after the peak seasons for the early-terminating, persistent and early-onset varieties are further discussed in section 6. Three events (1988, 1995 and 1998) appear to have the early-onset variety (Figure 2e).

The fourth variety is characterized by a sudden and late development of warm equatorial Atlantic SSTAs around June and is thus referred to as a late-onset variety (Figure 2d). The warm equatorial Atlantic SSTAs tend to persist relatively longer compared to the other varieties. Thus, precipitation over the West African sub-Sahel region is much enhanced for an extended period during July-October. Interestingly, however, precipitation over northeastern South America hardly changes during the late-onset variety. Six events (1949, 1951, 1968, 1981, 1993 and 2018) appear to display the late-onset variety (Figure 2e).

As shown in Figure S4, Sahelian rainfall over 10°N-20°N is generally reduced during June-September, thus weakening the West African summer monsoon (e.g., Vizy and Cook, 2002; Losada et al., 2010). The Sahelian rainfall reduction is more robust for the persistent and late-onset varieties, but much weaker for the early-onset variety. As shown in Figures S2 and S3, the four most frequently recurring Atlantic Niño varieties (Figure 2) are very well reproduced when the other two SST datasets are used. See Text S2 and Figures S4-S6 for additional analysis and discussion on the spatiotemporal diversity of Atlantic Niña.

4. Potential Onset Mechanisms of the Four Atlantic Niño Varieties

To better understand atmosphere-ocean dynamic processes linked to the onsets of the four Atlantic Niño varieties, we show maps of surface wind anomalies, SSHAs, and SSTAs regressed onto the four varieties for December-February (DJF [-1,0]), MAM [0], and JJA [0] (Figure 3); any month in the year prior to, during and after the Atlantic Niño year is denoted by the suffix (-1), (0) and (+1), respectively. For the early-terminating variety, a negative phase of Atlantic Meridional Mode (AMM) develops in DJF (-1,0) and MAM (0) with cold and warm SSTAs in the tropical North Atlantic (TNA) and tropical South Atlantic (TSA), respectively. The resulting cross-equatorial gradient of SSTAs drives interhemispheric wind anomalies (i.e., northeasterly in TNA and northwesterly in TSA) in MAM (0), which lead to a robust development of positive SSHAs and warm SSTAs in the eastern equatorial Atlantic in MAM (0) and JJA (0). Therefore, it appears that the early-terminating variety is driven by a negative phase of the AMM in boreal spring. This onset mechanism of Atlantic Niño was previously suggested by Foltz and McPhaden (2010). Additionally, the early-terminating variety appears to be similar to the so-called Horse-Shoe mode, for which upwelling Kelvin waves generated by Rossby wave reflection serve as the dissipation mechanism (Martin-Rey et al., 2019).

For the persistent variety, equatorial wind anomalies and SSHAs are very weak in DJF (-1,0) and MAM (0) and thus likely to contribute little to the onset. Instead, this mode is preconditioned by a robust weakening of the off-equatorial trade winds in both hemispheres during DJF (-1,0) and MAM (0), which leads to reduced evaporative cooling and warm SSTAs in the TNA and TSA regions in MAM (0). In addition, southwesterly wind anomalies off the coast of West Africa weaken coastal upwelling (evidenced by positive SSHAs), contributing to the gradual build-up of strong warm SSTAs in that area, known as Dakar Niño (Oettli et al., 2016). Richter et al. (2012) suggested that the anomalous warm surface water off the coast of West Africa could be advected to the equatorial Atlantic region to trigger and sustain this Atlantic Niño variety, which they referred to as the non-canonical Atlantic Niño.

The early-onset variety is characterized by an early development of warm SSTAs along the coast of Southwest Africa and the interior TSA (across 20°S) in DJF (-1,0). But, more importantly, it is preconditioned by persistent interhemispheric wind anomalies during DJF (-1,0) and MAM (0). It appears that these wind anomalies are directly responsible for a gradual and early development of warm equatorial Atlantic SSTAs. Therefore, both the early-onset and early-terminating varieties seem to be initiated by interhemispheric wind anomalies. Unlike the early-terminating variety, however, the TNA SSTAs during DJF (-1,0) and MAM (0) are very weak. This suggests that the persistent interhemispheric wind anomalies that are prevalent during the onset phase of the early-onset variety in DJF (-1,0) and MAM (0) may be sustained by external forcing. The external forcing that may trigger and sustain these interhemispheric wind anomalies is discussed in the next section. Another key difference between the early-terminating and early-onset varieties is the stronger eastward SSHA gradient along the equator in MAM (0) and JJA (0) for the early-terminating variety, which is consistent with Bjerknes feedback and the confinement of positive SSTAs to the eastern equatorial Atlantic. In contrast, the broader spatial distributions of positive SSTAs and SSHAs for the early-onset variety are suggestive of remote ENSO forcing (Chang et al., 2006), as discussed in the next section.

The late-onset variety is very distinct from the other three varieties because there is no clear preconditioning of SSTAs or surface wind anomalies in DJF (-1,0) or MAM (0). It develops spontaneously around May (0) and June (0) with no clear source of external forcing. Therefore, it appears that the late-onset variety develops through atmosphere-ocean processes internal to the equatorial Atlantic. A weak buildup of positive SSHA gradient along the equator in MAM (0) suggests that the eastward propagation of downwelling equatorial Kelvin waves and its amplification by Bjerknes feedback play an important role in the initiation of the late-onset variety, as previously suggested by Keenlyside and Latif (2007). If that is the case, the onset mechanism of the late-onset variety is most comparable to that of canonical El Niño in the Pacific.

5. Potential Influence of ENSO on the Onsets of Atlantic Niño Varieties

Figures 4a-d show the four most frequently occurring Atlantic Niño varieties and the associated equatorial Pacific SSTAs between July of the preceding year and June of the following year. The early-terminating variety is linked to slightly cold SSTAs in the equatorial Pacific during the preceding boreal winter (Figure 4a). This means that La Niña events may occasionally precede this Atlantic Niño variety but are not necessarily required for it to develop in boreal summer. As shown in Figures 4b and 4c, it is clear that both the persistent and early-onset varieties are linked to strong El Niño events during the preceding boreal winter, suggesting that they are largely forced by El Niño events.

To better understand how some El Niño events may trigger the persistent and early-onset varieties, Figures 4e-h show velocity potential and divergent wind anomalies at 200 hPa, and mean sea level pressure and surface wind anomalies in DJF (-1,0) regressed onto the two varieties. In both cases, the tropical Atlantic region is characterized by anomalous subsidence, which is a typical response to El Niño-induced warming of the tropical Atlantic troposphere and associated increase in atmospheric static stability (e.g., Horel and Wallace, 1981; Yulaeva and Wallace, 1994; Mestas-Nuñez and Enfield, 2001; Chiang and Sobel, 2002). For the early-onset variety, the anomalous subsidence is largely north of the equator. Due to the anomalous sinking and increased static stability, the vertical development of convection is suppressed. Therefore, high sea level pressure anomalies are formed over TNA to sustain the interhemispheric wind anomalies. For the persistent variety, on the other hand, anomalous subsidence is stronger and covers a much broader region in the tropical Atlantic. As such, the trade winds are greatly weakened in both TNA and TSA, which in turn warms both TNA and TSA in boreal spring (MAM). However, no clear interhemispheric wind anomalies are formed across the equator. As suggested by Richter et al. (2012), the anomalously warm surface water off the coast of West Africa could be carried by ocean currents to the equatorial Atlantic region to trigger the Atlantic Niño. Although the atmospheric flow anomalies linked to the two varieties are statistically distinctive (Figure S8), it is unclear why some strong El Niño events are linked to the persistent variety and others the early-onset variety. It is uncertain if this difference is due to El Nino diversity or processes internal to Atlantic.

6. Concluding Remarks

By performing a spatiotemporal EOF analysis of observed Atlantic Niño events, we identify the four most frequently recurring Atlantic Niño varieties. The first two contrast the timing of dissipation (i.e., early-terminating versus persistent varieties), while the other two the timing of onset (i.e., early-onset versus late-onset varieties). Largely consistent with the timings of onset and dissipation, the four varieties display remarkable differences in climate response over the surrounding continents. In particular, the persistent and late-onset varieties correspond to an extended period of increased rainfall over the West African sub-Sahel region during June-October, while the early-terminating and early-onset varieties correspond to a limited period of increased rainfall over the West African sub-Sahel region during June-August or July-August. Similarly, rainfall over northeastern South America tends to increase during the peak seasons of the early-terminating, persistent and early-onset Atlantic Niño varieties. However, rainfall in this region is not strongly modified during the late-onset variety. Rainfall anomalies over northeastern South America prior to or after the peak seasons are most likely driven by either the AMM for the early-terminating variety (Foltz et al., 2012) or ENSO in the Pacific for the persistent and early-onset varieties (e.g., Hastenrath and Heller, 1977).

Further regression analysis suggests that each of the four Atlantic Nino varieties is subject to clearly different onset mechanisms. The early-terminating variety is preconditioned and triggered by a negative phase of the AMM in boreal spring (e.g., Foltz and McPhaden, 2010). Both the persistent and early-onset varieties appear to be forced by strong El Niño events in the preceding boreal winter. The persistent variety seems to be initiated by oceanic advection of warm SSTAs off the coast of West Africa (Richter et al., 2012). The early-onset variety appears to be largely forced by interhemispheric wind anomalies that are persistently forced during DJF and MAM by El Niño-induced anomalous subsidence and increased sea level pressure over TNA. In contrast to the other three varieties, the late-onset variety is spontaneously triggered by atmosphere-ocean processes internal to the equatorial Atlantic (e.g., Keenlyside and Latif, 2007) and shows no clear source of external forcing in boreal spring, thus suggesting low seasonal predictability compared to the other three varieties.

Acknowledgements

We thank the Editor Suzana Camargo and two anonymous reviewers for insightful comments and suggestions. This work was carried out during I.V.C.'s visit to NOAA's Atlantic Oceanographic and Meteorological Laboratory (AOML) as a student intern. I.V.C. thanks Claudia

Schmid, Gustavo Goni, Hosmay Lopez and Jay Harris for their help and support during his internship at NOAA/AOML, and Marta Martin-Rey for her helpful comments and suggestions. This work was supported by the Spanish Government funding through projects VA-DE-RETRO (CTM2014-56987-P) and SAGA (RTU2018-100844-B-C33), and by NOAA's Climate Program Office, Climate Variability and Predictability Program (award GC16-207) and NOAA/AOML. I.V.C. was funded through FPI contract (BES-2015-071314). The HadISST1 were provided by UK Met Office at https://www.metoffice.gov.uk/hadobs/hadisst. The NCEP-NCAR reanalysis, the NOAA gauge observation-based global land precipitation reconstruction dataset, the COBE and the ERSST5 were provided by NOAA/ESRL/PSD at http://www.esrl.noaa.gov/psd. ORAS4 were provided by the Copernicus Marine Environment Monitoring Service (CMEMS) at ftp://ftp-icdc.cen.uni-hamburg.de/EASYInit/ORA-S4/monthly_1x1.

References

Balmaseda, M. A., Mogensen, K. and Weaver, A. T. (2013). Evaluation of the ECMWF ocean reanalysis system ORAS4. *Q. J. R. Meteorol. Soc.*, 139, 1132 - 1161. https://doi.org/10.1002/qj.2063.

Brandt, P., Funk, A., Hormann, V., Dengler, M., Greatbatch, R. J., and Toole, J. M. (2011). Interannual atmospheric variability forced by the deep equatorial Atlantic Ocean. *Nature*, *473*(7348), 497 - 500. https://doi.org/10.1038/nature10013.

Burmeister, K., Brandt, P. and Lübbecke, J. F. (2016). Revisiting the cause of the eastern equatorial Atlantic cold event in 2009. *J. Geophys. Res.*, *121*(7), 4777 - 4789. https://doi.org/10.1002/2016jc011719.

Carton, J. A., and Huang, B. (1994). Warm events in the tropical Atlantic. *J. Phys. Oceanogr.*, *24*, 888 - 903.

Chang, P., Fang, Y. Saravanan, R., Ji, L., and Seidel, H. (2006). The cause of the fragile relationship between the Pacific El Niño and the Atlantic Niño. *Nature*, *443*(7109), 324 - 328. https://doi.org/10.1038/nature05053.

Chen, M., Xie, P. Janowiak, J. E., and Arkin, P. A. (2002). Global land precipitation: A 50-yr monthly analysis based on gauge observations. *J. Hydrometeorol.*, *3*, 249 - 266.

Chiang, J. C. H., and Sobel, A. H. (2002). Tropical tropospheric temperature variations caused by ENSO and their influence on the remote tropical climate. *J. Climate*, *15*, 2616 - 2631.

Florenchie, P., C. Reason, J. C., Lutjeharms, J. R. E., Rouault, M., Roy, C. and Masson, S. (2004). Evolution of interannual warm and cold events in the Southeast Atlantic Ocean, *J. Climate*, *17*(12), 2318 - 2334.

Folland, C. K., Colman, A. W. Rowell, D. P. and Davey, M. K. (2001). Predictability of northeast Brazil rainfall and real-time forecast skill, 1987-98. *J. Climate*, *14*(9), 1937 - 1958.

Foltz, G., Brand, P. et al., (2019). The tropical Atlantic observing system. *Front. Mar. Sci.*, *6*, 206. https://doi.org/10.3389/fmars.2019.00206.

Foltz, G. R., and McPhaden, M. J. (2010). Interaction between the Atlantic meridional and Niño modes. *Geophys. Res. Lett.*, *37*(18), L18604, https://doi.org/10.1029/2010gl044001.

Foltz, G.R., McPhaden, M. J., and Lumpkin, R. (2012). A strong Atlantic meridional mode event in 2009: The role of mixed layer dynamics. *J. Climate*, *25*, 363 - 380, https://doi.org/10.1175/JCLI-D-11-00150.1.

Giannini, A. (2003). Oceanic forcing of Sahel rainfall on interannual to interdecadal time scales, *Science*, *302*(5647), 1027 - 1030. https://doi.org/10.1126/science.1089357.

Gill, A. E., (1980). Some simple solutions for heat-induced tropical circulation. *Quart. J. Roy.*

Meteor. Soc., *106*, 447 - 462.

Hastenrath, S. and Heller, L. (1977). Dynamics of climatic hazards in northeast Brazil. *Q.J.R. Meteorol. Soc.*, *103*, 77 - 92. https://doi .org/10.1002/qj.49710343505.

Horel, J. D., and Wallace, J. M. (1981). Planetary-scale atmospheric phenomena associated with the Southern Oscillation. *Mon. Wea. Rev.*,*109*, 813 - 829.

Huang, B., Thorne, P. W. et al., (2017). Extended Reconstructed Sea Surface Temperature version 5 (ERSSTv5), Upgrades, validations, and intercomparisons. *J. Climate*, *30*, 8179 - 8205. https://doi.org/10.1175/JCLI-D-16-0836.1.

Ishii, M., Shouji, A., Sugimoto, S., and Matsumoto, T. (2005). Objective analyses of sea-surface temperature and marine meteorological variables for the 20th century using ICOADS and the Kobe collection. *Int. J. Climatol.*, *25*, 865 - 879.

Jouanno, J., Hernandez, O, and Sanchez-Gomez, E. (2017). Equatorial Atlantic interannual variability and its relation to dynamic and thermodynamic processes. *Earth Syst. Dynam.*, *8*, 1061 - 1069. https://doi.org/10.5194/esd-8-1061-2017.

Kalnay, E. et al. (1996). The NCEP/NCAR 40-year reanalysis project. *Bull. Amer. Meteor. Soc.*, *77*(3), 437 - 471.

Keenlyside, N. S., and Latif, M. (2007). Understanding equatorial Atlantic interannual variability. *J. Climate*, *20*(1), 131 - 142. https://doi.org/10.1175/jcli3992.1.

Kucharski, F., Bracco, A., Yoo, J. H., and Molteni, F. (2008). Atlantic forced component of the Indian monsoon interannual variability. *Geophys. Res. Lett.*, 35, L04706, https://doi.org/10.1029/2007GL033037.

Latif, M., and Grötzner, A. (2000). The equatorial Atlantic oscillation and its response to ENSO. *Clim. Dyn.*, *16*(2-3), 213 - 218.

Lee, S.-K., Dinezio, P. N., Chung, E.-S., Yeh, S.-W., Wittenberg, A. T., and Wang, C. (2014). Spring persistence, transition, and resurgence of El Niño. *Geophys. Res. Lett.*, *41*(23), 8578 - 8585. https://doi.org/10.1002/2014gl062484.

Lee, S.-K., Lopez, H., Chung, E.-S., DiNezio, P. N., Yeh, S.-W. and Wittenberg, A. T. (2018). On the fragile relationship between El Nino and California rainfall. *Geophys. Res. Lett.*, *45*, 907 - 915. https://doi.org/10.1002/2017GL076197.

Losada, T., Rodríguez-Fonseca, B., Janicot, S. et al. (2010). A multi-model approach to the Atlantic Equatorial mode: Impact on the West African monsoon. *Clim. Dyn. 35*, 29 - 43. https://doi.org/10.1007/s00382-009-0625-5.

Lübbecke, J. F., Rodríguez-Fonseca, B., Richter, I., Martín-Rey, M., Losada, T., Polo, I., and Keenlyside, N. S. (2018). Equatorial Atlantic variability-modes, mechanisms, and global teleconnections. *WIREs Climate Change*, *9*(4). https://doi.org/10.1002/wcc.527.

Lübbecke, J. F., and Mcphaden, M. J. (2012). On the inconsistent relationship between Pacific and Atlantic Niños. *J. Climate*, *25*(12), 4294 - 4303. https://doi.org/10.1175/jcli-d-11-00553.1.

Lübbecke, J. F., and Mcphaden, M. J. (2013). A comparative stability analysis of Atlantic and Pacific Niño modes. *J. Climate*, *26*, 5965 - 5980. https://doi.org/10.1175/JCLI-D-12-00758.1.

Lübbecke, J. F., Böning, C. W., Keenlyside, N. S., and Xie, S.-P. (2010). On the connection between Benguela and equatorial Atlantic Niños and the role of the South Atlantic Anticyclone. *J. Geophys. Res.*, *115*(C9). https://doi.org/10.1029/2009jc005964.

Lübbecke, J. F., Burls, N. J. Reason, C. J. C. and Mcphaden, M. J. (2014). Variability in the South Atlantic anticyclone and the Atlantic Niño mode. *J. Climate*, *27*(21), 8135 - 8150. https://doi.org/10.1175/jcli-d-14-00202.1.

Martín-Rey, M., Polo, I., Rodríguez-Fonseca, B., Losada, T. and Lazar, A. (2018). Is there evidence of changes in tropical Atlantic variability modes under AMO phases in the observational record? *J. Climate*, *31(2)*, 515 - 536. https://doi.org/10.1175/JCLI-D-16-0459.1.

Martín-Rey, M., Polo, I., Rodríguez-Fonseca, B., Lazar, A., & Losada, T. (2019). Ocean dynamics shapes the structure and timing of Atlantic Equatorial Modes. *J. Geophys. Res.*, *124*, 7529 - 7544. https://doi.org/10.1029/2019JC015030.

Mestas-Nuñez, A. M. and Enfield, D. B. (2001). Eastern equatorial Pacific SST variability: ENSO and non-ENSO components and their climatic associations. *J. Climate*, *14*, 391 - 402,

Nnamchi, H. C., Li, J. Kucharski, F., Kang, I.-S., Keenlyside, N. S., Chang, P. and Farneti, R. (2016). An equatorial–extratropical dipole structure of the Atlantic Niño. *J. Climate*, *29*(20), 7295 - 7311. https://doi.org/10.1175/jcli-d-15-0894.1.

Nnamchi, H. C., Li, J. Kucharski, F., Kang, I.-S., Keenlyside, N. S., Chang, P. and Farneti, R. (2015). Thermodynamic controls of the Atlantic Niño. *Nat. Commun.*, *6*(1). https://doi.org/10.1038/ncomms9895.

Oettli, P., Morioka, Y. and Yamagata, T. (2016). A regional climate mode discovered in the North Atlantic: Dakar Niño/Niña. *Sci. Reports, 6*, 18782.

Okumura, Y., and Xie, S.-P. (2004). Interaction of the Atlantic equatorial cold tongue and the African monsoon. *J. Climate*, *17*, 3589 - 3602.

Okumura, Y., and Xie, S.-P. (2006). Some overlooked features of tropical Atlantic climate leading to a new Niño-like phenomenon. *J. Climate*, *19*(22), 5859 - 5874. https://doi.org/10.1175/jcli3928.1.

Philander, S. G. H. (1986). Unusual conditions in the tropical Atlantic Ocean in 1984, *Nature*, *322*(6076), 236 - 238. https://doi.org/10.1038/322236a0.

Pottapinjara, V., G. M. S, Murtugudde, R., Ashok, K., and Ravichandran, M. (2019). On the relation between boreal spring position of Atlantic inter-tropical convergence zone and Atlantic zonal mode. *J. Climate*, *32*, 4767 - 4781. https://doi.org/10.1175/jcli-d-18-0614.1.

Rayner, N. A., Parker, D. E., Horton, E. B., Folland, C. K., Alexander, L. V., Rowell, D. P. Kent, E. C. and Kaplan, A. (2003). Global analyses of sea surface temperature, sea ice, and night marine air temperature since the late nineteenth century. *J. Geophys. Res.*, *108*, 4407. https://doi.org/10.1029/2002JD002670.

Richter, I., Behera, S. K., Masumoto, Y., Taguchi, B. Sasaki, H. and Yamagata T. (2012). Multiple causes of interannual sea surface temperature variability in the equatorial Atlantic Ocean. *Nat. Geosci.*, *6*(1), 43 - 47. https://doi.org/10.1038/ngeo1660.

Shannon, L. V., Boyd, A. J., Brundrit, G. B., and Taunton-Clark, J. (1986). On the existence of an El Niño-type phenomenon in the Benguela System. *J. Mar. Res.*, *44*(3), 495 - 520. https://doi.org/10.1357/002224086788403105.

Tokinaga, H., Richter, I., and Kosaka, Y. (2019). ENSO influence on the Atlantic Niño, revisited: Multi-year versus single-year ENSO events. *J. Climate*, *32*, 4585 - 4600. https://doi.org/10.1175/jcli-d-18-0683.1.

Tschakert, P., Sagoe, R., Ofori-Darko, G., and Codjoe, S. N. (2010). Floods in the Sahel: an analysis of anomalies, memory and anticipatory learning. *Climatic Change*, 103, 471 - 502. https://doi.org/10.1007/s10584-009-9776-y.

Vizy, E. K., and Cook, K. H. (2002). Development and application of a mesoscale climate model for the tropics: Influence of sea surface temperature anomalies on the West African monsoon. *J. Geophys. Res.*, *107*, https://doi.org/10.1029/2001JD000686.

Yulaeva, E., and Wallace, J. M. (1994). The signature of ENSO in global temperature and precipitation fields derived from the microwave sounding unit. *J. Climate*, *7*, 1719 - 1736

Zebiak, S. E. (1993). Air–Sea interaction in the equatorial Atlantic region. *J. Climate*, *6*(8), 1567 - 1586.

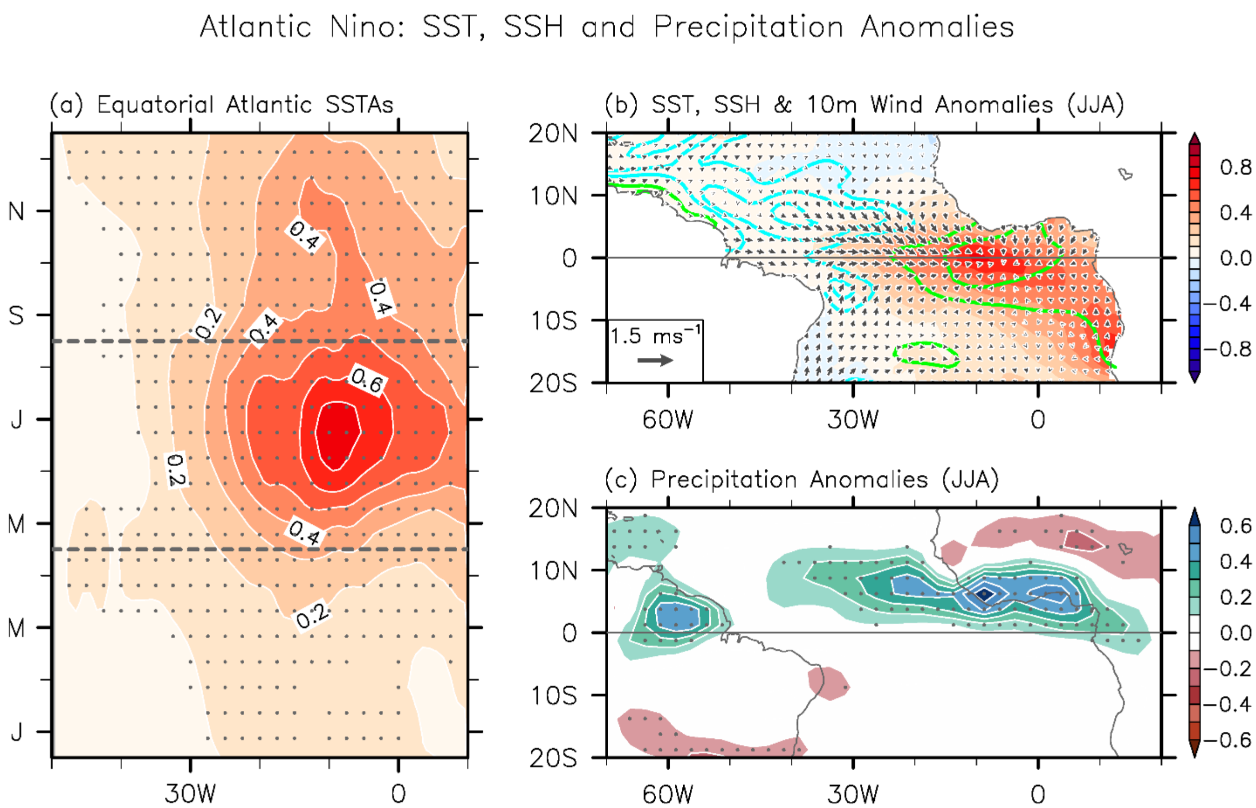

Figure 1. (a) Time-longitude plot of composite mean equatorial Atlantic SSTAs, averaged between 3°S and 3°N, from January to December derived from observed Atlantic Niño events. Significant SSTA values at 99% or above based on a Student's t-test (two tailed) are indicated by gray dots. (b) Composite mean tropical Atlantic SST (shades), SSH (contours) and 10-m wind (vectors) anomalies, and (c) precipitation anomalies during June-August derived from observed Atlantic-Niño events. Positive and negative SSHAs are indicated by green and cyan contour lines, respectively in (b). Significant precipitation anomaly values at 95% or above based on a Student's t-test (two tailed) are indicated by gray dots in (c). The units for SST, SSH, winds and precipitation are in °C, m s^{-1} cm, and mm day^{-1}, respectively. The contour interval for SSH anomalies is 0.5 cm.

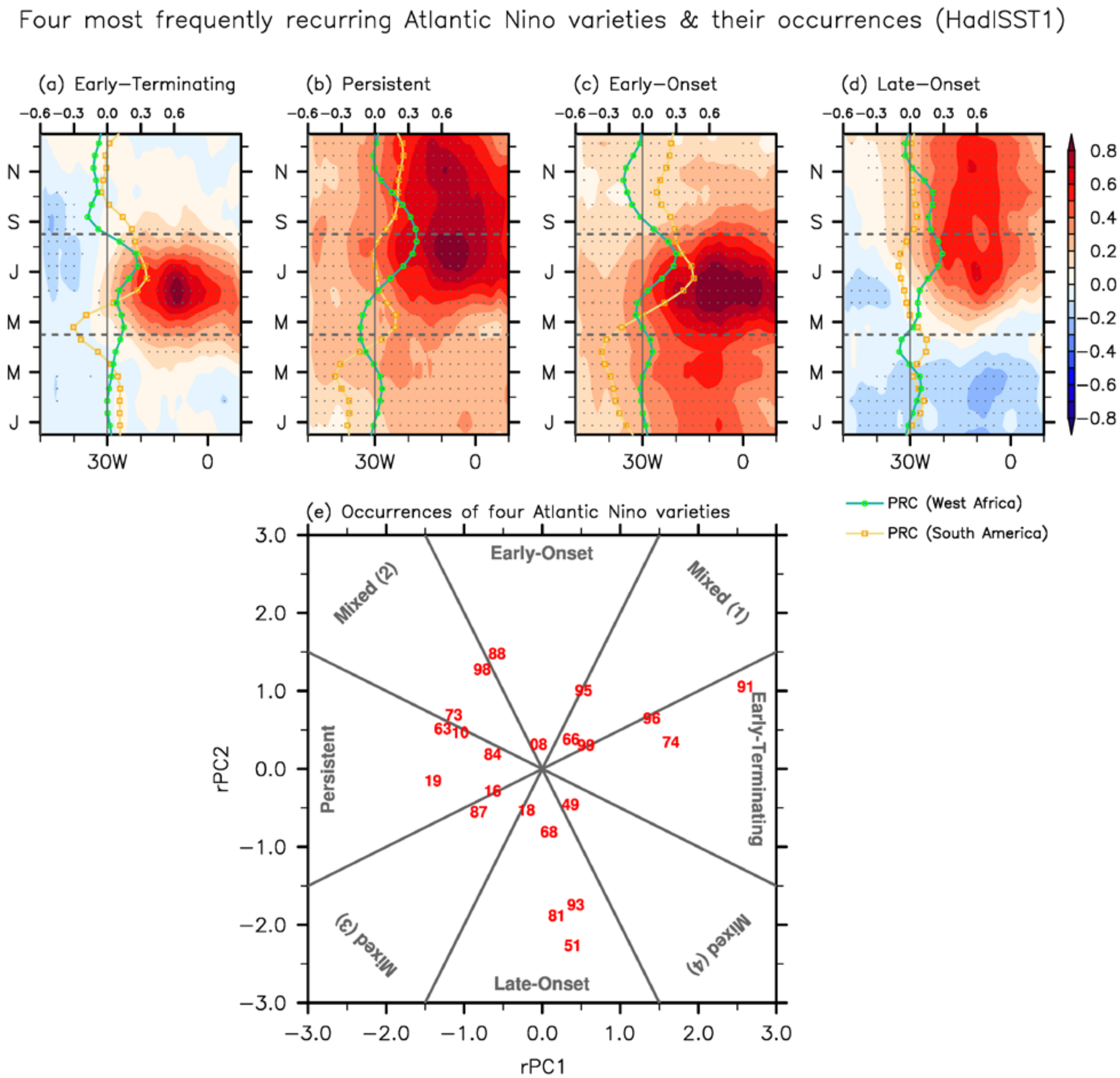

Figure 2. (a–d) Time-longitude plots of the tropical Atlantic SSTAs (averaged over 3°S-3°N; shades) illustrate the four most frequently recurring Atlantic Niño varieties during 1948–2019, namely, (a) the early-terminating, (b) persistent, (c) early-onset, and (d) late-onset varieties. Significant SSTA values at 99% or above based on a Student's t-test (two tailed) are indicated by gray dots. Land precipitation anomalies over South America (averaged over 0°-10°N and 70°W-50°W; orange lines) and West African sub-Sahel region (averaged over 0°-10°N and 20°W-20°E; green lines) are also shown for each of the four Atlantic Niño varieties. (e) Normalized rotated

PC1 versus rotated PC2 values for all 22 events. The two-digit numbers indicate the Atlantic Niño years. The dashed gray lines in Figures 2a–2c indicate May 1 and August 31. The thick gray lines in Figure 2e are the boundaries (i.e., rPC1 = $\pm 2 \times$ rPC2 and rPC2 = $\pm 2 \times$ rPC1) that separate the four varieties from the mixed varieties. The units for SST and precipitation are in °C and mm day^{-1}, respectively.

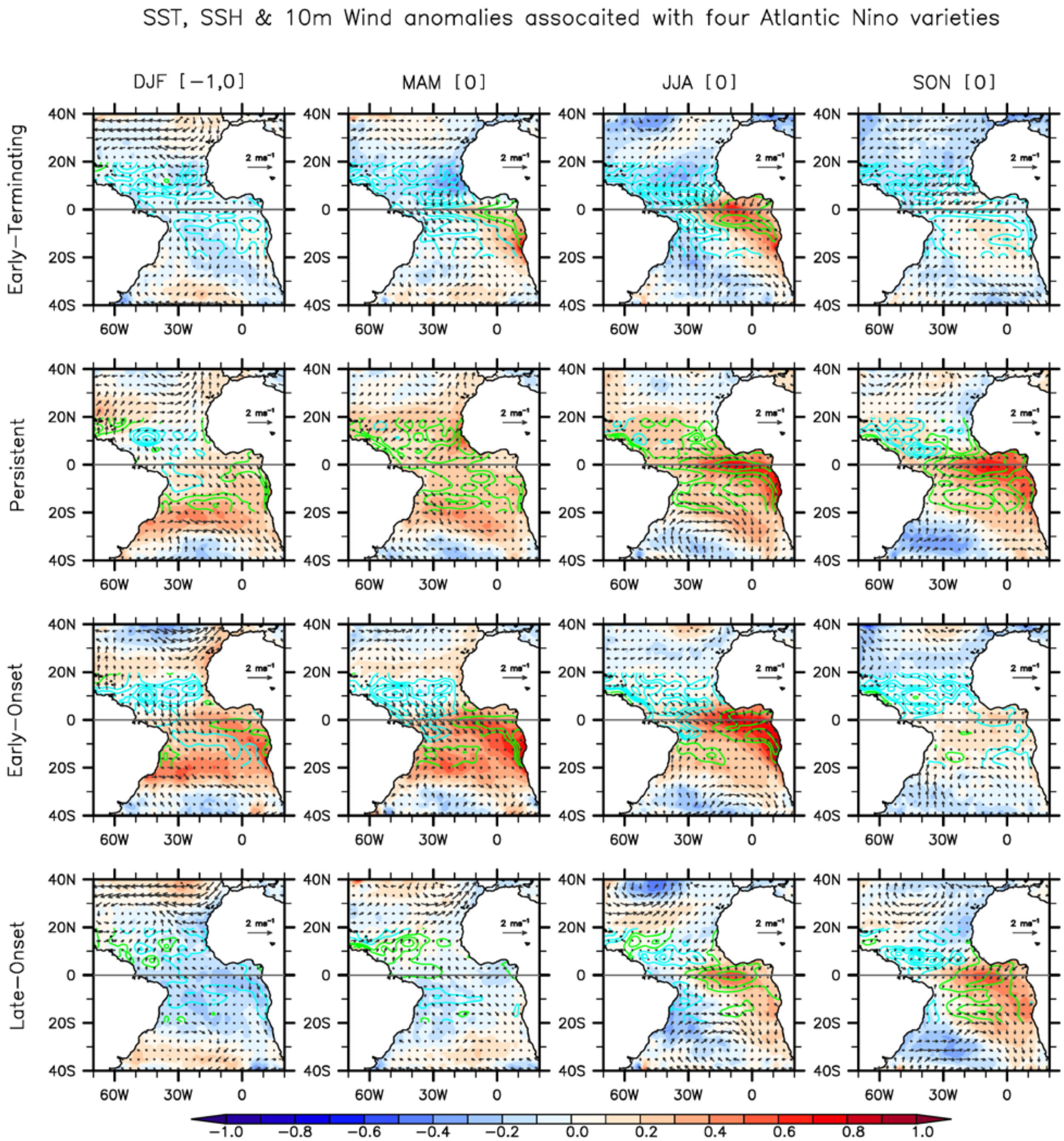

Figure 3. SST (shaded), SSH (contours) and 10 m wind (vectors) anomalies regressed onto the four Atlantic Niño varieties for (1st row) December-February (DJF [-1,0]), (2nd row) MAM [0], (3rd column) JJA [0] and (4th row) SON [0]. Positive and negative SSHAs are indicated by green and cyan contour lines, respectively. The units for SST, SSH and winds are in °C, cm, and m s^{-1}, respectively. The contour interval for SSH anomalies is 0.5 cm.

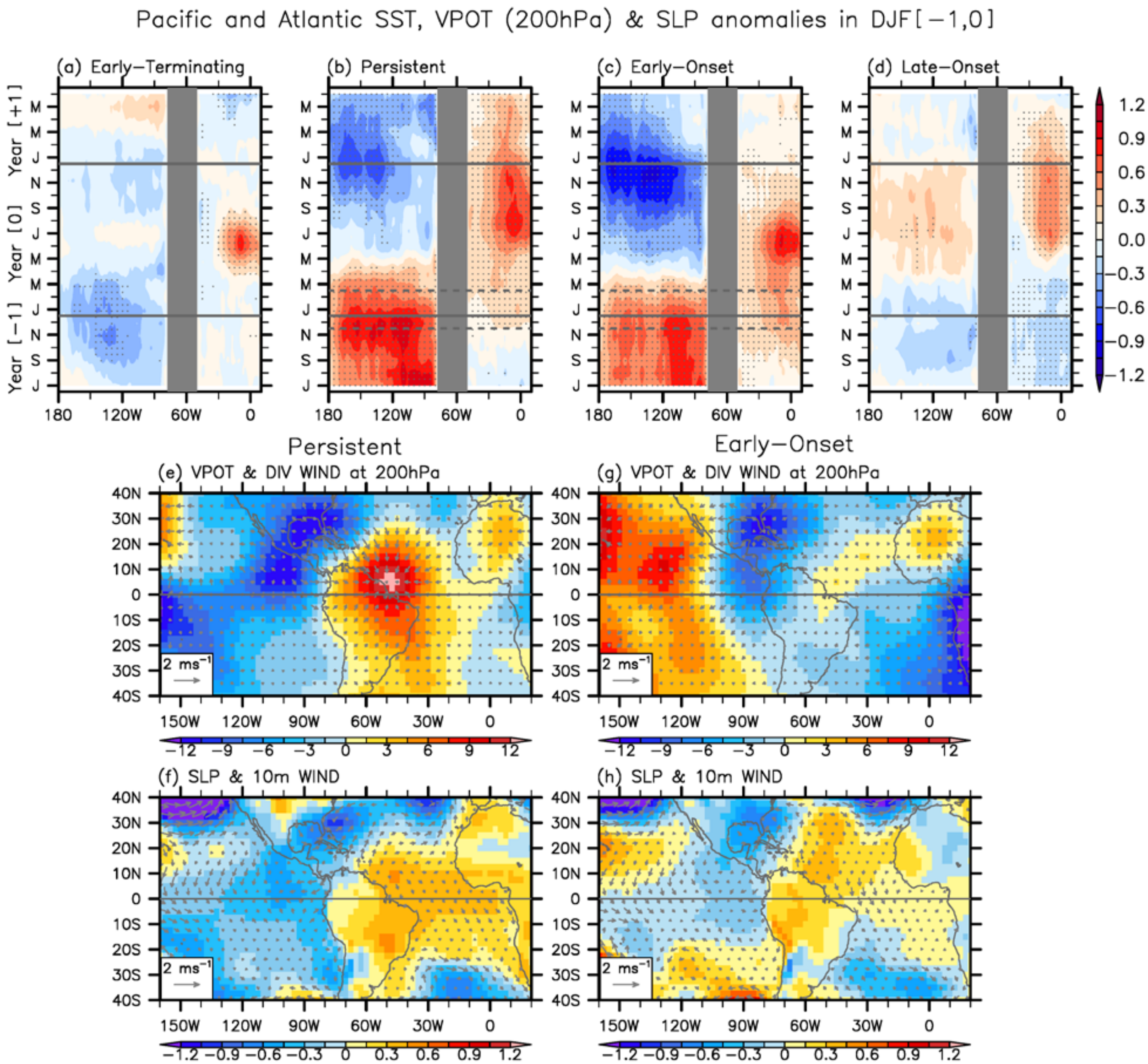

Figure 4. (a-d) Time-longitude plots of the tropical Pacific SSTAs (averaged over 5°S-5°N) and tropical Atlantic SSTAs (averaged over 3°S-3°N) for the four most frequently recurring Atlantic Niño varieties spanning from July (-1) to June (+1). Significant SSTA values at 99% or above based on a Student's t-test (two tailed) are indicated by gray dots. (e,g) Velocity potential (shades) and divergent wind anomalies (vectors) at 200 hPa and (f,h) mean sea level pressure (shades) and surface (10 m) wind anomalies (vectors) in DJF (-1,0) regressed on (e,f) the persistent and (g,h) early-onset varieties. The units for SST, velocity potential, sea level pressure and winds are in °C,

10^{-7} m^2 sec^{-1}, hPa and m s^{-1}, respectively.